Synergistic Enhancement of H_2 and CH_4 Evolution by CO_2 Photoreduction in Water with Reduced Graphene Oxide−Bismuth Monoxide Quantum Dot Catalyst

Songmei Sun,*,† Motonori Watanabe,† Pangpang Wang,‡ and Tatsumi Ishihara*,†

†International Institute for Carbon-Neutral Energy Research (I2CNER), Kyushu University, Fukuoka 819-0395, Japan

‡Nanomaterials Laboratory, Institute of System, Information Technologies and Nanotechnologies, Fukuoka 819-0388, Japan

* Supporting Information

ABSTRACT: Photocatalytic water splitting or CO_2 reduction is one of the most promising strategies for solar energy conversion into hydrogen-containing fuels. However, these two processes typically compete with each other, which significantly decreases the solar energy conversion efficiency. Herein, we report for the first time this competition can be overcome by modulation of reactive sites and electron transfer pathway of heterogeneous photocatalysts. As a prototype, BiO composite reduced graphene oxide quantum dots (RGO-BiO QDs) were synthesized, which can provide large amounts of photogenerated electrons as well as individual reactive sites for H^+ and CO_2 reduction. The productivity of H_2, CH_4, and CO by the RGO-BiO QDs catalyst were 102.5, 21.75, and 4.5 μmol/(g·h), respectively, in pure water without the assistance of any cocatalyst or sacrificial agent. The apparent quantum efficiency at 300 nm reached to 4.2%, which is more than 10 times higher than that of RGO-TiO_2 QDs (0.28%) under the same conditions. In situ DRIFT, ESR, and photoelectrochemical studies confirmed that the unique circled electron transfer pathway (E_{vb}(BiO) → E_{cb}(BiO) → E_f(RGO) → $E_{V_O\bullet}$(BiO)) and the large amount of separated different reactive sites are responsible for the highly efficient simultaneous H_2 evolution and CO_2 reduction performance.

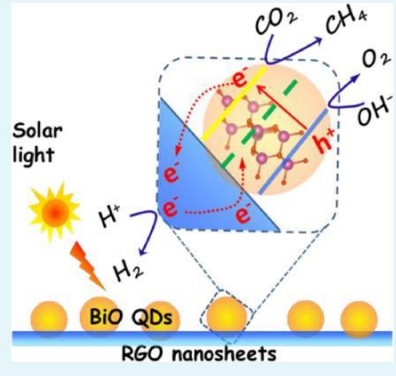

KEYWORDS: carbon dioxide reduction, pure water splitting, photocatalysis, solar energy conversion, oxygen vacancy

INTRODUCTION

Solar energy conversion to chemical fuels by photocatalytic water splitting or CO_2 reduction is a promising strategy to solve the problems of the energy crisis.[1−4] However, the conversion efficiency by photocatalysis from solar energy to products is still unsatisfactory and requires further increase for commercialization. It is generally recognized that H_2 evolution competes with CO_2 reduction in the photocatalytic process because the reduction of H^+ to H_2 is kinetically more favorable.[5−7] Realization of efficient H_2 evolution and CO_2 reduction simultaneously on one catalyst is a great challenge. There is no successful report of such up to the present.

Compared with conventional bulk or nanoscale materials, quantum-sized semiconductors have the most potential to realize this target. First, quantum-sized semiconductors have higher surface areas to provide more reactive sites.[8] The redox potential of photogenerated charge carriers in quantum-sized semiconductors can typically be improved by the quantum confinement effect, which facilitates the photochemical reactions.[9−11] In addition, multiple exciton generation in quantum-sized semiconductors usually increases the concentration of photogenerated charge carriers compared with that of conventional materials.[12,13] However, quantum-sized semiconductors also have a disadvantage in that the space charge layers are not effective for the separation of electron−hole pairs,[14] which is one of the main reasons that quantum-sized semiconductors for efficient water splitting or CO_2 reduction are rarely reported. Besides the charge carrier behavior, the active site is another important factor that influences the photocatalytic activity. Under a high concentration of photogenerated electrons, the catalyst must provide sufficient reactive sites for H_2 evolution and CO_2 reduction. It is difficult to construct different active sites in a single catalyst; therefore, the development of a composite photocatalyst with much improved electron−hole separation and multiple diverse reactive sites is highly desirable.

Among the various material options for the preparation of a composite photocatalyst, graphene with a sp^2-hybridized two-dimensional carbon structure may be the most appropriate. Graphene composite materials typically exhibit high activity due to much improved electron−hole separation. Many graphene composited materials such as TiO_2,[15] CdS,[16] C_3N_4,[17] Cu_2O,[18] and some perovskite semiconductors[19] have demonstrated improved activity for water splitting or CO_2 reduction.[20] However, the state-of-the-art performance of these photocatalysts for H_2 evolution from pure water splitting is

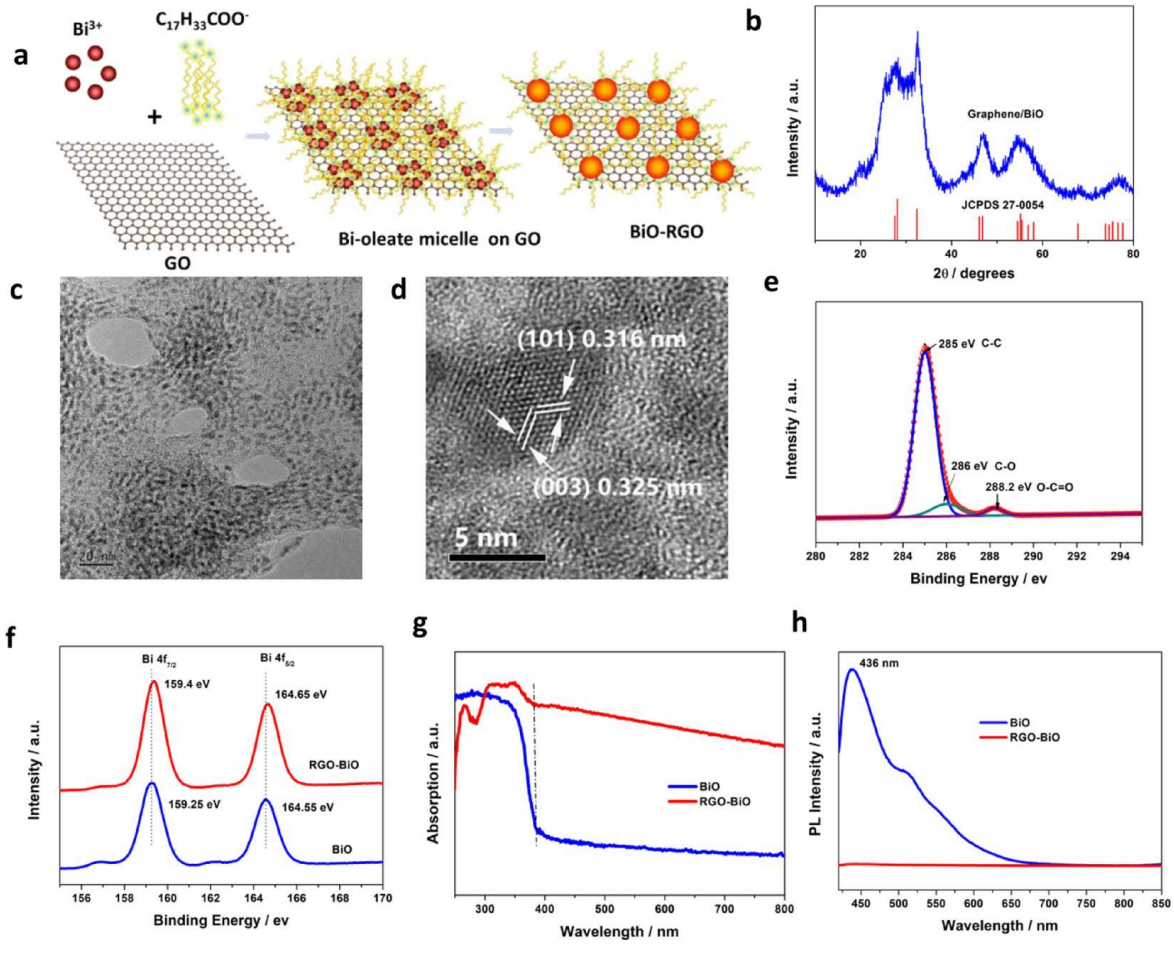

Figure 1. Characterizations for the hydrothermally synthesized RGO-BiO sample. (a) Schematic illustration for in situ growth BiO QDs on RGO nanosheet by the assistant of oleate ions. (b) XRD pattern of the as-prepared RGO-BiO QDs nanocomposite. (c) TEM image of the as-prepared RGO-BiO QDs. (d) HRTEM image of the RGO-BiO QDs. (e) C 1s XPS spectrum for RGO-BiO QDs. (f) Bi 4f XPS spectra for RGO-BiO QDs and pure BiO QDs samples. (g) UV−vis diffuse reflection spectra of the samples. (h) Room temperature PL spectra of RGO-BiO QDs and pure BiO QDs powders excited at 350 nm.

only ~70 μmol/(g·h) under the assistance of Pt in the Z-scheme,[21] and that for CO_2 reduction is typically below 10 μmol/(g·h) for CH_4 generation,[22] which is far lower than that required for practical application. No graphene composite photocatalyst for both improvement of H_2 evolution and CO_2 reduction has been developed to date. Recently, Hu et al. reported that protons can be quickly transported in monolayer graphene.[23] This study inspired us to design a graphene composite photocatalyst to separate the reactive sites for H^+ and CO_2 reduction by modulation of the electron-transfer pathway and reactive sites to realize the synergistic enhancement of H_2 evolution and CO_2 reduction to improve the solar energy conversion efficiency. This process also requires a high concentration of photogenerated charge carriers and different separated reactive sites. Fabrication of a graphene composite quantum-sized photocatalyst is highly imperative to achieve synergistic enhancement of H_2 evolution and CO_2 reduction target based on the proposed concept.

In this work, nanocomposites of bismuth monoxide quantum dots (BiO QDs) decorated reduced graphene oxide (RGO) nanosheets are constructed for the first time to study the possibility of efficient simultaneous H_2 evolution and CO_2 reduction during simulated solar light driven photocatalytic process. We chose BiO catalyst because it has a unique electronic structure in which lone pair electrons existed around the bivalent bismuth element, providing strong electron donating power for adsorption and activation of insert molecules which has been proved in our previous studies.[24] Combining the excellent proton transfer property of RGO and the unique electronic structure of BiO, the RGO-BiO QDs catalyst may realize efficient photocatalytic performance on simultaneous H_2 evolution and CO_2 reduction in one catalytic process.

RESULTS AND DISCUSSION

To obtain a tightly composited material, an in situ crystallization process was designed for preparing RGO-BiO QDs composite material by the hydrothermal synthesis approach (Figure 1a; detailed information in the Supporting Information). The X-ray diffraction (XRD) pattern of the RGO-BiO QDs sample (Figure 1b) can be indexed to the hexagonal phase of BiO [space group R3m (160), JCPDS No. 27-0054] with an average grain size of ca. 2.7 nm based on the Scherrer equation. Besides, the peak around 20.3 is the (002) diffraction peak of RGO. The low-magnification transmission electron microscopy (TEM) image in Figure 1c shows the BiO QDs uniformly spread over the surface of the RGO sheets. The high-resolution TEM (HRTEM) image (Figure 1d) indicates

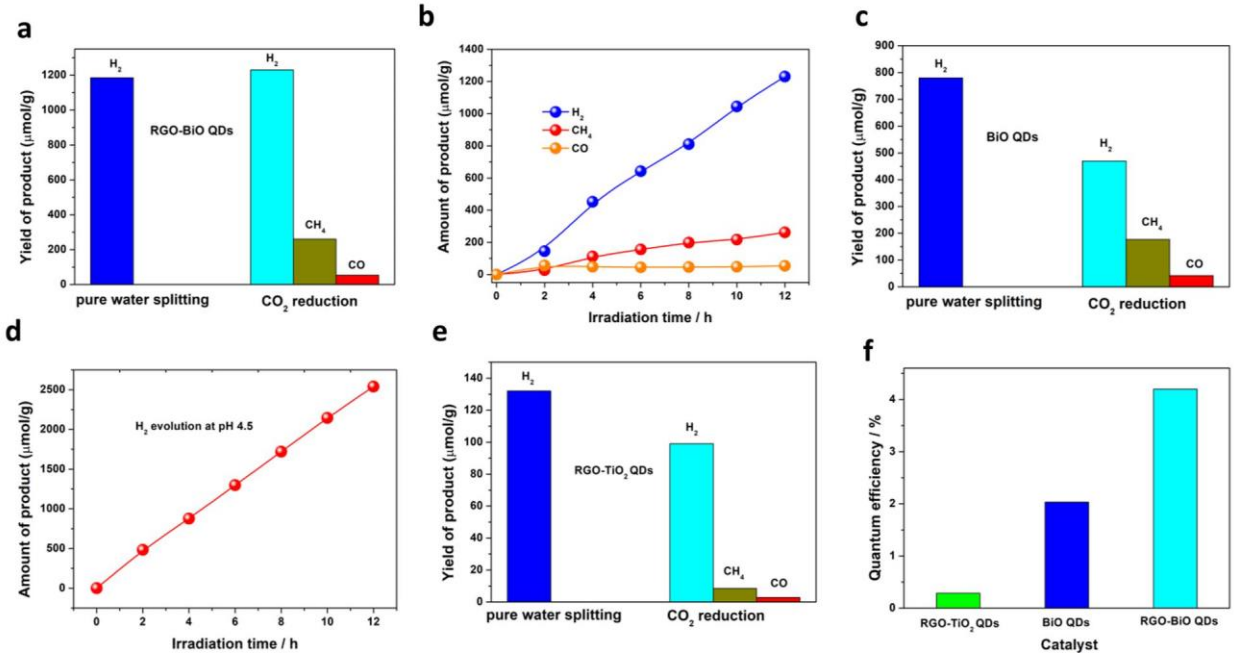

Figure 2. Photocatalytic performances of the as-prepared different samples under simulated solar light irradiation. (a) Photocatalytic performance of RGO-BiO QDs for pure water splitting and CO_2 reduction after 12 h of photocatalytic reaction. (b) H_2, CH_4, and CO evolution from the RGO-BiO catalyst as a function of the irradiation time in the CO_2 reduction experiment. (c) Photocatalytic performance of pure BiO QDs for pure water splitting and CO_2 reduction after 12 h of photocatalytic reaction. (d) H_2 evolution by water splitting over RGO-BiO QDs under acid conditions. (e) Photocatalytic performance of RGO-TiO_2 QDs for pure water splitting and CO_2 reduction after 12 h of photocatalytic reaction. (f) Apparent quantum efficiency of different samples under 300 nm light irradiation.

lattice planes with d-spacings of ca. 0.316 and 0.325 nm, which further confirmed the excellent crystallinity of the BiO QDs. For comparative study, pure BiO QDs were also prepared under the same conditions without the addition of GO. XRD measurement and TEM observation (Figure S1) proved the pure BiO QDs possess a similar grain size and morphology as that anchored on RGO.

To investigate the chemical interaction between the BiO QDs and RGO nanosheets as well as the reduction degree of GO in the hydrothermal process, high resolution X-ray photoelectron spectroscopy (XPS) were collected. Figure 1e shows the C 1s spectrum for the RGO-BiO QDs nanocomposite, which can be deconvoluted into three smaller peaks: sp^2-bonded carbon (C−C, 284.8 eV), epoxy/hydroxyls (C−O, 286.9 eV), and carboxyl (O−C O, 288.7 eV). The reduction degree of GO in RGO-BiO QDs nanocomposite can be quantified by calculating the relative content of carbon in the sample. According to their peak areas, there was 88% graphitic carbon and 12% oxidized carbon in the RGO-BiO QDs, which indicates a high degree of GO reduction after the hydrothermal process. The C 1s and O 1s XPS spectra of pure GO after a similar hydrothermal process without the addition of Bi were also conducted for comparative study. As shown in Figure S2a, the reduction degree of GO can be calculated to be about 85%, which is very close to the value calculated from RGO-BiO sample (88%). Figures S2b−d show the O 1s XPS spectrum of RGO-BiO QDs, pure RGO, and pure BiO QDs, respectively. It was found the peak of O 1s from RGO (531.2, 532.6 eV in Figure S2b) in the RGO-BiO QDs sample shifted to lower binding energy position compared with that in the pure RGO (531.4, 532.8 eV in Figure S2c). On the contrary, the peak of O 1s from BiO (530.1, 531.3 eV in Figure S2b) in the RGO-BiO QDs sample shifted to higher binding energy position compared with that in the pure BiO (530, 531.2 eV in Figure S2d). Figure 1f shows the Bi 4f XPS spectrum of the pure BiO QDs and RGO-BiO QDs samples. Compared with that in pure BiO, the Bi 4f XPS spectrum of the RGO-BO QDs showed an obvious shift to higher binding energy. All of these XPS spectra indicate a chemical interaction existed between the RGO and BiO QDs by Bi−O bond. This chemical interaction was further proved by Raman spectrum of RGO and RGO-BiO QDs composites. As shown in Figure S3, significant structural changes occurred after the BiO QDs decorated on RGO sheets. In the Raman spectrum of RGO-BiO QDs, both D band and G band of RGO were broadened when compared with that in the pure RGO sample. The G band of RGO in RGO-BiO QDs shifted to 1596 cm^{-1}, while it is located at 1585 cm^{-1} in pure RGO. As is well-known, the D band response originated from the edges which can be attributed to either defects or the breakdown of translational symmetry, while the G band corresponds to the first-order scattering of the E_{2g} mode of the sp^2 domain of graphite.[25,26] The Raman shift of the G band for RGO in RGO-BiO QDs sample provides reliable evidence for the chemical interaction between the RGO plane surface and BiO QDs. Moreover, it was found the relative intensity of the D band compared to the G band in the RGO-BiO QDs sample (ID/IG = 1.44) is very close to that in pure RGO (ID/IG = 1.38), indicating chemical composition with BiO QDs did not obviously increase the defect sites in RGO.

The optical properties of the as-prepared catalyst were studied using UV−vis absorption and photoluminescence (PL) spectroscopy. As shown in Figure 1g, the RGO-BiO QDs and pure BiO QDs sample exhibited a similar light absorption band edge. However, an intense background was observed in RGO-BiO QDs sample, which is due to the absorption from

aggregated solid state RGO powder. PL spectroscopy was then employed to examine the fates of photoexcited charge carriers in these photocatalysts. As shown in Figure 1h, supra-band gap irradiation (wavelength = 350 nm) of BiO QDs results in a strong emission of photons at around 436 nm, which is ascribed to either direct band gap or indirect band gap recombination of the photogenerated charge carriers. Under the same conditions, complete PL quenching was observed for the RGO-BiO QDs sample, indicating much improved electron−hole separation in the composite material.

The photocatalytic performance of RGO-BiO QDs sample was investigated by CO_2 reduction and pure water splitting experiments performed in a sealed Pyrex bottle under a 300 W Xe arc lamp irradiation. For CO_2 reduction, the main products are H_2, CH_4, and CO which were detected by gas chromatography. Besides, trace amounts of CH_3CH_2OH and CH_3COOH can also been observed in the reaction solution from ^1H NMR. In this study, we only use the main products to evaluate the photocatalytic performance.

Figure 2a summarizes the amounts of H_2, CH_4, and CO produced after 12 h of photocatalytic reaction for pure water splitting and CO_2 reduction by the RGO-BiO QDs sample. The evolved H_2 and CH_4 in CO_2 reduction experiment by the RGO-BiO QDs sample increased almost linearly with irradiation time (Figure 2b). Besides, it was found the amount of H_2 produced in CO_2 reduction experiment was not decreased and even slightly higher than that from pure water splitting under the same conditions (Figure 1a), indicating a noncompetitive H^+ and CO_2 reduction process. In the CO_2 reduction experiment on the RGO-BiO QDs sample, the calculated productivity for H_2, CH_4, and CO is 102.5, 21.75, and 4.5 μmol/(g·h), respectively. According to the consumed electrons for H_2, CH_4, and CO generation, the turnover number of the RGO-BiO catalyst in CO_2 reduction experiment is calculated to be 1.05 within 12 h, indicating a catalytic process. O_2 evolution during the photocatalytic water splitting and CO_2 reduction was also tested by the RGO-BiO QDs catalyst, which is about 37 and 84 μmol/(g·h) (Figure S4) for pure water splitting and CO_2 reduction, respectively. Compared with the theoretical value, the slightly lower O_2 evolution amount may be originated from the hole oxidation of surface oleate ions, which will be discussed in detail in the following section.

For comparison, the photocatalytic performance of pure BiO QDs and pure RGO was also investigated under the same conditions. As shown in Figure 2c, H_2 evolution from CO_2 reduction (39 μmol/(g·h)) on pure BiO QDs is obviously decreased when comparing with that from pure water splitting (65 μmol/(g·h)) along with a decreased CH_4 (14.75 μmol/(g· h)) and CO (3.5 μmol/(g·h)) production. This result indicates H^+ and CO_2 reduction compete with each other on the pure BiO QDs catalyst, which is similar to most of the previously reported photocatalysts. There is no H_2 and CH_4 product that can be detected by using pure RGO as catalyst under the same photocatalytic conditions.

The noncompetitive water splitting and CO_2 reduction performance of RGO-BiO QDs catalyst demonstrated at least two important points. One is that the quantity of the photogenerated electrons in RGO-BiO QDs sample is much higher than the H^+ concentration in the pure water splitting reaction solution. To prove this, we conducted a H_2 evolution experiment in an acid condition (pH 4.5) in an Ar-saturated reaction cell. It was found H_2 evolution over the RGO-BiO QDs catalyst increased linearly with the irradiation time and reached a high productivity of 2540 μmol/g within 12 h (Figure 2d), indicating the high concentration of photo-generated electrons in the RGO-BiO QDs catalyst. Another important point revealed from the photocatalytic results of RGO-BiO QDs sample is that the main reactive sites for H^+ and CO_2 reduction may be separated because the H_2 evolution efficiency is not affected in CO_2 reduction experiment.

We investigated whether the noncompetitive water splitting and CO_2 reduction process is general in RGO composited semiconductor quantum dots catalyst. TiO_2 quantum dots decorated RGO nanosheets were also prepared for comparative study. Figure S5 shows the TEM image of our prepared RGO-TiO_2 QDs catalyst, from which one can see that the TiO_2 quantum dots with an average size of 3−6 nm were uniformly dispersed on RGO sheets. The photocatalytic performances of the RGO-TiO_2 QDs catalyst for pure water splitting and CO_2 reduction are summarized in Figure 2e, from which one can see H_2 evolution and CO_2 reduction also competed with each other in the RGO-TiO_2 QDs catalyst. Besides, it was found the selectivity of the photogenerated electrons for CO_2 reduction is severely decreased to 27%. This value is 47% in the RGO-BiO QDs sample under the same conditions. The apparent quantum efficiencies of the different photocatalysts for CO_2 reduction were also detected under a 300 nm band filter, which is 4.2%, 2%, and 0.28% (Figure 2f) for RGO-BiO QDs, BiO QDs, and RGO-TiO_2 QDs sample, respectively.

To confirm that the produced CH_4 in RGO-BiO QDs catalyst indeed come from CO_2 reduction rather than from oleate contaminants or RGO, we performed two parallel experiments. First, we measured the blank photocatalytic experiment in an Ar atmosphere over RGO-BiO QDs catalyst without using CO_2 under the same conditions. After irradiation for 12 h, no CH_4 was detected. After that, we performed an isotopic experiment with $^{13}CO_2$ as the initial reactant under the same photocatalytic reaction conditions. The resultant photocatalytic products were detected by gas chromatography−mass spectrometry (GC-MS). Because of the relatively low concentration of CO in the final product, only the $^{13}CH_4$ peak was observed in GC-MS. In the mass spectrum extracted from GC-MS analysis (Figure S6), the molecular ion peak with an m/z value of 17 is attributed to $^{13}CH_4$. These studies clearly show that the CH_4 product indeed comes from CO_2 reduction.

To investigate the photostability of the RGO-BiO QDs sample for CO_2 reduction, we conducted the CO_2 reduction experiment in a prolonged irradiation time. The reaction vessel filled with pure CO_2 was initially irradiated for 12 h at 4 °C and then opened under the same temperature in air. After 5 min, the reaction vessel was closed, refilled with pure CO_2, and continued to be irradiated under a Xe arc lamp at 4 °C. This process was repeated four times. The obtained photocatalytic performance is shown in Figure S7a. From Figure S7a, it can be see that H_2 evolution rate is well maintained within the first two cycles and decreased from the third cycle. However, the CH_4 evolution rate gradually decreased from the first to the fourth cycle. The decreased H_2 and CH_4 evolution rates were ascribed to the formation of the $(BiO)_2CO_3$ species (Figure S7b) on the catalyst surface. Along with the formation of $(BiO)_2CO_3$, the QD particles were grown and connected with each other on the RGO sheets (Figure S8). The formation of $(BiO)_2CO_3$ species may be ascribed to the elimination of surface oleate ions during the photocatalytic process. The

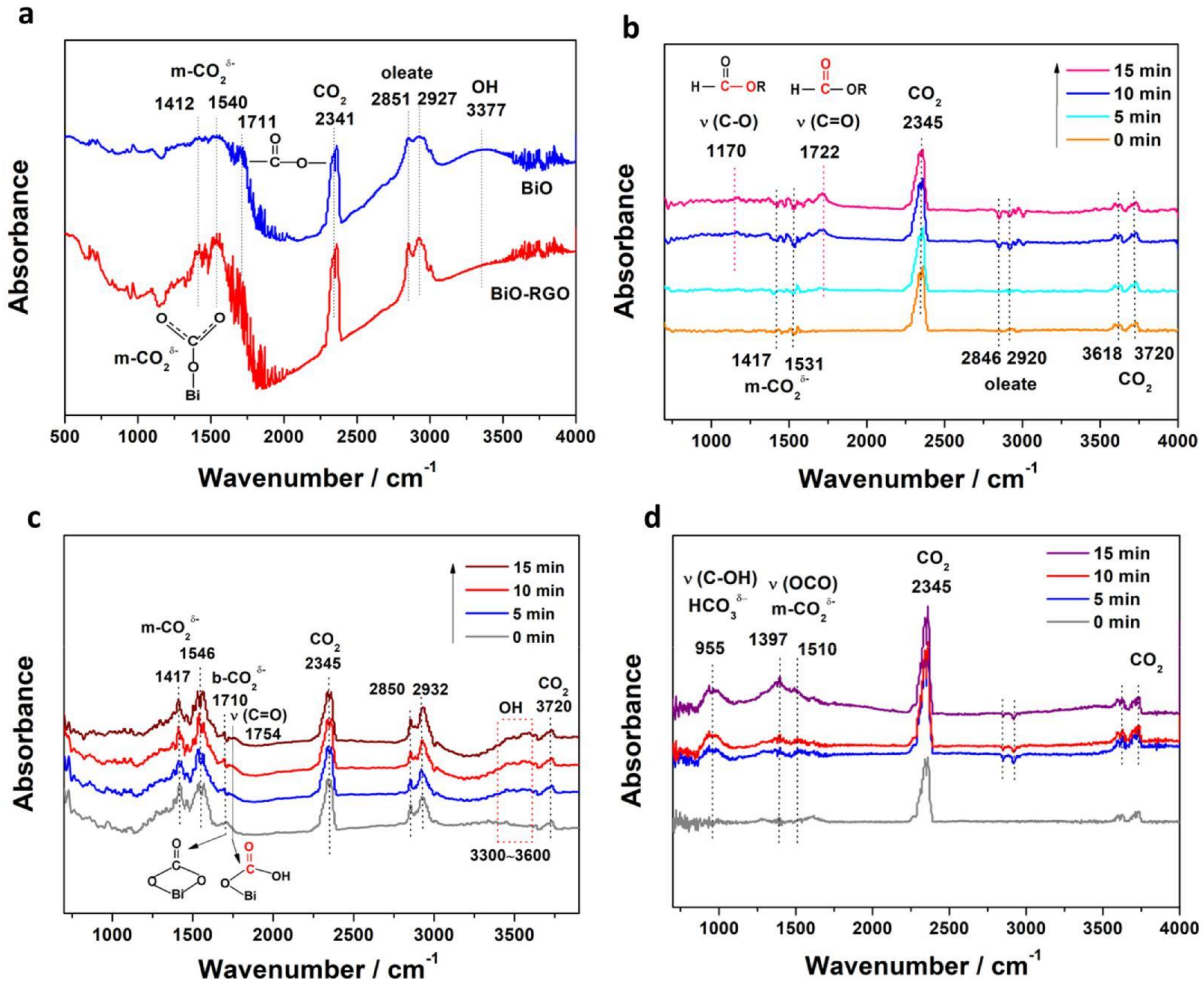

Figure 3. CO_2 adsorption and activation on different samples revealed by DRIFT. (a) DRIFT spectra of the RGO-BiO QDs and pure BiO QDs sample under vacuum in the dark. (b) In situ DRIFT spectra recorded after ambient temperature adsorption of CO_2/H_2O on RGO-BiO QDs under 300 W Xe arc lamp irradiation. (c) In situ DRIFT spectra recorded after ambient temperature adsorption of CO_2/H_2O on pure BiO QDs under 300 W Xe arc lamp irradiation. (d) In situ DRIFT spectra recorded after ambient temperature adsorption of CO_2/H_2O on commercial Bi_2O_3 under 300 W Xe arc lamp irradiation.

RGO-BiO QDs surface is protected by a large amount of oleate ions initially. During a photocatalytic process, these oleate ions were gradually oxidized by photogenerated holes [BiO(h^+)] under light irradiation, which is confirmed by DRIFT of the RGO-BiO sample before under after photo-catalytic reaction (Figure S9). Because of high concentration of CO_3^{2-} ions in the reaction solution, once there is not enough oleate ions protecting the surface, CO_3^{2-} ions will react with BiO (h^+) immediately to form $(BiO)_2CO_3$ species on the catalyst surface. CO_3^{2-} corrosion and passivation is a general problem for metal oxide catalyst in CO_2 or O_2 reduction process which requires further studies in the future.

The main interesting question raised in this research is why the RGO-BiO QDs catalyst exhibits synergistic enhancement of H_2 and CH_4 evolution in CO_2 reduction. To investigate the mechanism, CO_2 adsorption and activation process on the as-prepared catalyst were studied using in situ diffuse reflectance infrared Fourier transform spectroscopy (DRIFT). Before introducing CO_2, DRIFT spectra for BiO QDs and RGO-BiO QDs catalysts in the vacuum state were analyzed at first. Figure 3a shows the RGO-BiO QDs and pure BiO QDs catalysts have a similar DRIFT spectrum on CO_2 adsorption, indicating that CO_2 molecules may be mainly adsorbed on the BiO surface in the RGO-BiO catalyst. A characteristic absorption band of linear CO_2 was observed at 2341 cm^{-1} on both pure BiO and RGO-BiO catalyst, which corresponds to the asymmetrical stretching vibration of CO_2. This CO_2 absorption peak in the vacuum state is ascribed to the preadsorbed CO_2 in air which is difficult to be desorbed only under the vacuum state at room temperature. Different from gas-phase CO_2, the flexural vibration peak (666 cm^{-1}) of adsorbed CO_2 almost disappeared (Figure 3a), along with the appearance of three new absorption bands around ~1412, 1540, and 1711 cm^{-1}. The absorption bands around ~1412 and ~1540 cm^{-1} are attributed to the symmetric stretching and asymmetric OCO stretching modes of monodentate carbonate species, m-$CO_2^{\delta-}$, the carbon atoms of which interact with the surface oxygen of the catalyst.[27−29] The absorption band at ~1711 cm^{-1} is caused by the C O stretching vibration from an OCOOR (where R represents a Bi atom) bidentate carbonate (b-$CO_2^{\delta-}$) species.[30,31] The absorption bands around 2851 and 2972 cm^{-1} come from surface residual oleate ions. Compared with the RGO-BiO QDs sample, a broad absorption band around 3377 cm^{-1} was also observed for the pure BiO QDs sample, which is ascribed to the O−H stretching vibration.[6] This indicates that the surface of the pure BiO QDs sample is

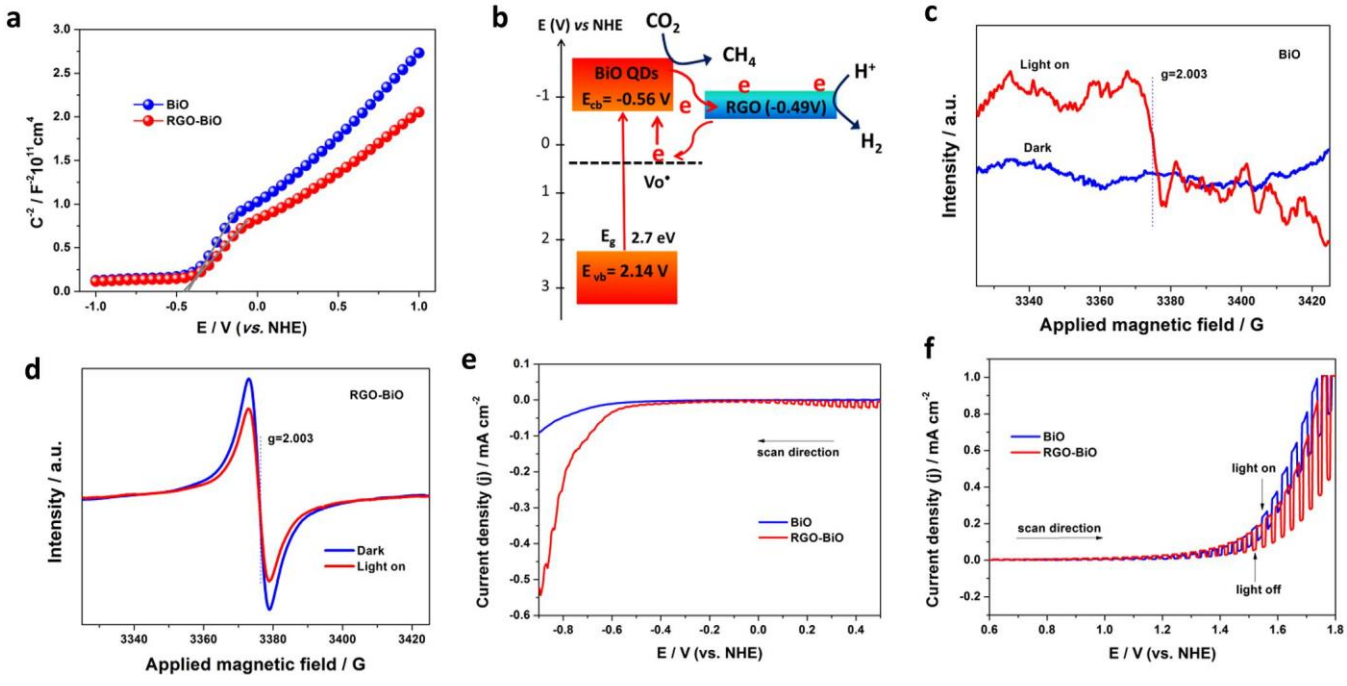

Figure 4. Possible electron transfer pathway and improved electron concentration in RGO-BiO QDs investigated by ESR and electrochemical measurement. (a) Mott−Schottky plots of the as-prepared RGO-BiO QDs and BiO QDs electrodes in 0.1 M Na_2SO_4. (b) Schematic energy level diagram and electron transfer pathway in RGO-BiO QDs composite for CO_2 and H^+ reduction. (c) ESR spectrum of pure BiO QDs with and without light irradiation at 165 K in N_2. (d) ESR spectrum of RGO-BiO QDs nanocomposite with and without light irradiation at 165 K in N_2. (e) Cathodic current−potential scans of the synthesized samples in 0.1 mol L^{-1} Na_2SO_4 under 300 W chopped Xe arc lamp irradiation. (f) Anodic current−potential scans of the synthesized samples in 0.1 mol L^{-1} Na_2SO_4 under 300 W chopped Xe arc lamp irradiation.

more hydrophilic than the RGO-BiO QDs composite. There is no characteristic DRIFT absorption band observed for RGO in the RGO-BiO QDs sample because the C C vibration (1590−1620 cm^{-1}) was overlapped by the strong absorption from $CO_2^{\delta-}$ carbonate species (1420−1700 cm^{-1}).[27,32]

To further investigate the CO_2 reduction process on the catalyst surface, in situ DRIFT measurement was conducted after exposing the RGO-BiO QDs catalyst to CO_2/H_2O mixed gas at room temperature under 300 W Xe arc lamp irradiation. As shown in Figure 3b, the DRIFT absorption from m-$CO_2^{\delta-}$ on the RGO-BiO QDs sample was gradually decreased under light irradiation. Two new absorption bands appeared at around 1170 and 1722 cm^{-1}, which correspond to the stretching vibrations of C−O and C O in the HCOOR species, respectively.[33,34] This suggests that m-$CO_2^{\delta-}$ species on the RGO-BiO QDs surface were hydrogenated into HCOOR (R = H or Bi) intermediate species under light irradiation, which are then transformed into CO or CH_4 in the subsequent photocatalytic processes. Different from the RGO-BiO sample, the m-$CO_2^{\delta-}$ species did not contribute significantly to the final CO_2 reduction performance of pure BiO sample. After introducing CO_2/H_2O molecules on the DRIFT cell, although two increased absorption bands from m-$CO_2^{\delta-}$ were clearly observed on the BiO QDs surface, their absorption intensities were almost unchanged after light irradiation, indicating the m-$CO_2^{\delta-}$ species is difficult to be further reduced by the pure BiO QDs catalyst. On the contrary, the OCOOR b-$CO_2^{\delta-}$ species on the pure BiO catalyst surface were found obviously decreased and trans-formed into OCOOH under light irradiation (Figure 3c). Therefore, the final CH_4 product from pure BiO QDs comes from the reduction of the OCOOH intermediate. Besides, a broad absorption band around 3300−3600 cm^{-1} appeared on the pure BiO QDs surface after light irradiation, which corresponds to the stretching vibration of O−H. This OH group originated from water dissociation on the pure BiO QDs surface. The increased absorption band of the OH group was not observed in the RGO-BiO sample from the DRIFT spectrum after light irradiation, further proved the reactive site for water splitting by RGO-BiO is on RGO. In situ DRIFT measurement of a commercial Bi_2O_3 photocatalyst was also conducted under the same conditions for comparison. Figure 3d shows that although the m-$CO_2^{\delta-}$ and $HCO_3^{\delta-}$ species were increased under light irradiation on the Bi_2O_3 surface, these species were not further transformed with the prolonged irradiation time. In addition, no CH_4 or CO products from CO_2 reduction over commercial Bi_2O_3 were observed under the same photocatalytic conditions, which further demon-strates the importance of the active sites in the BiO catalyst for CO_2 adsorption and activation.

Besides the excellent CO_2 activation on BiO surface in the RGO-BiO composite, another reason for the synergistic enhancement of H_2 and CH_4 evolution by the RGO-BiO QDs catalyst may be ascribed to a unique electron transfer pathway between BiO and RGO under light irradiation, which finally separates the main reactive sites for H^+ and CO_2 reduction. To investigate the possible electron transfer pathway in the RGO-BiO QDs composite material, electro-chemical measurements were conducted on different catalyst films.

Figures 4a shows the Mott−Schottky spectrum of the as-prepared RGO-BiO QDs and BiO QDs samples, which is usually used for the analysis of the flat band potential (E_{fb}) of semiconductor electrodes. The E_{fb} value calculated from the intercept of the axis with potential values was at −0.46 and −0.43 V vs NHE for RGO-BiO QDs and BiO QDs,

respectively. For many n-type semiconductors, E_{fb} is considered to be about 0.1 V below the conduction band (E_{cb}).[35] Based on this, the estimated E_{cb} value of the RGO-BiO QDs and BiO QDs samples were −0.56 and −0.53 V vs NHE at pH 7. Previous studies have reported the Fermi level (E_f) of graphene was around −0.49 V vs NHE at pH 7.[36] Because of the lower energy level of E_f(RGO), electron transfer will occur from BiO to graphene when they are in contact under light irradiation (Figure 4b). This electron transfer process was experimentally monitored using the electron spin resonance (ESR) spectrum in this study. Before analyzing the ESR spectrum, it is worth noting that ESR can only detect unpaired electrons. Therefore, intrinsic $Vo^{\bullet\bullet}$ in pure BiO QDs are nonresponsive in ESR (Figure 4c). Under light (λ = 380 nm) irradiation, electrons were excited from E_{vb} to E_{cb} or $E_{Vo^{\bullet\bullet}}$. Meanwhile, some of the electrons in E_{cb} can hop to the lower $E_{Vo^{\bullet\bullet}}$ band. Both of the E_{cb} to $E_{Vo^{\bullet\bullet}}$ or E_{vb} to $E_{Vo^{\bullet\bullet}}$ electron transfer process under light irradiation can generate single-electron-trapped oxygen vacancy ($Vo^{\bullet}$, effective charge +1).[37] The observed increased $Vo^{\bullet}$ signal (g = 2.003) in the ESR spectrum (Figure 4c) under light irradiation confirmed this electron transfer process. Different from the pure BiO QDs catalyst, the RGO-BiO QDs sample exhibited an intense intrinsic single-electron-trapped $Vo^{\bullet}$ signal before light irradiation (Figure 4d). These Vo trapped electrons may be ascribed to π-electron injection from RGO during the material preparation process. After irradiation under monochromatic light (λ = 380 nm) for 1 min, the $Vo^{\bullet}$ signal in the RGO-BiO QDs sample dramatically decreased (Figure 4d) due to the formation of double-electron-trapped oxygen vacancies (Vo^{x}, effective charge 0). Considering the $Vo^{\bullet}$ energy position (usually 0.75 eV upward toward the E_{cb}),[37] $Vo^{\bullet}$ trapped electrons are possibly transferred from E_{cb}/E_{vb} of BiO QDs or RGO. Figure 4c indicates there is only a small enhancement of $Vo^{\bullet}$ signal by the electron transfer from E_{cb} or E_{vb} to $E_{Vo^{\bullet\bullet}}$ in pure BiO QDs sample under light irradiation. Therefore, the much decreased $Vo^{\bullet}$ signal (60 times higher than that increased in Figure 4c under light) in RGO-BiO QDs sample under light irradiation mainly comes from the electron transfer from RGO to $Vo^{\bullet}$ (BiO). Compared with electron transfer from semiconductor to RGO, back electron transfer from RGO to semiconductor was rarely reported because of the lack of energy levels for electron acception in ordinary semi-conductors. Here, the large amount of $Vo^{\bullet}$ in BiO provides the possibility of electron transfer via E_{vb}(BiO) → E_{cb}(BiO) → E_f(RGO) → $E_{Vo\bullet}$(BiO) (as shown in Figure 4b). Along this electron transfer pathway, CO_2 and H^+ reduction successively occurred on BiO and RGO surface, respectively. This conclusion can be proved by in situ DRIFT and electron chemical study. As mentioned above, the in situ DRIFT spectrum (Figure 3) has confirmed CO_2 reduction and water splitting process mainly proceed on the BiO QDs and RGO surface, respectively, in the RGO-BiO QDs catalyst. To further study the H^+ reduction kinetics, electrochemical measurement was conducted on BiO QDs and RGO-BiO QDs electrode. Figure 4e shows cathodic I−V curves of the different samples under chopped light irradiation in 0.1 M Na_2SO_4 (saturated by N_2). It was found the overpotential for water reduction on RGO-BiO QDs nanocomposite (−0.57 V vs NHE) under light irradiation decreased much compared with that on pure BiO QDs (−0.74 V vs NHE), which confirmed H^+ reduction proceeds more easily on RGO composited material because of the lower activation barrier for electron transfer from RGO to H^+. Besides, it was found both the photocathode (Figure 4e) and photoanode current density (Figure 4f) of the RGO-BiO QDs are almost 4−5 times higher than that of BiO QDs sample under the same voltage, proving the high concentration of photogenerated electrons in the RGO-BiO QDs sample.

Based on the above studies, the photocatalytic process of the BiO QDs and RGO-BiO QDs catalyst is illustrated in Figure S10 to show why the RGO-BiO QDs catalyst can realize highly efficient H_2 evolution and CO_2 reduction simultaneously. As shown in Figure S10a, upon solar light irradiation, electrons excited from E_{vb} to E_{cb} of BiO QDs catalyst. These E_{cb} electrons can transfer to the surface adsorbed m-$CO_2^{\delta-}$ species to form HCOOR (R = H or Bi) intermediates for CO_2 reduction. Meanwhile, a considerable amount of photo-generated electrons in E_{cb} of RGO-BiO QDs transferred to the RGO sheet due to its lower E_f level. Because of the excellent electron/proton transfer property of RGO and the lower activation barrier of electron transfer from RGO to H^+ (Figure 4e), H_2 evolution from H^+ reduction preferentially proceeds on the RGO surface. H_2 evolution experiment under acidic conditions has confirmed that the quantity of photo-generated electrons in RGO-BiO QDs catalyst is sufficiently high for driving both H^+ and CO_2 reduction in pure water. Therefore, a considerable amount of electrons can transfer back to $Vo^{\bullet}$ active sites on BiO QDs surface after H^+ reduction. This electron back transfer can increase the electron concentration for CO_2 reduction on BiO QDs surface and then increase the CO_2 reduction selectivity. These advantages of RGO-BiO QDs catalyst lead to the rarely observed synergistic enhancement of H_2 and CH_4 evolution in CO_2 photoreduction experiment. For pure BiO QDs catalyst, H^+ and CO_2 reduction competed on BiO surface (Figure S10b), exhibiting a relatively low H_2 evolution rate in the presence of CO_2.

CONCLUSIONS

In summary, synergistic enhancement of H_2 evolution and CO_2 reduction was realized for the first time by modulation of the reactive sites and electron transfer pathway of a heterogeneous photocatalyst. For RGO-BiO QDs nano-composite catalyst as an example, the photocatalytic productivity of H_2, CH_4 and CO from CO_2 reduction in pure water was up to 102.5, 21.75, and 4.5 μmol/(g·h), respectively, without the assistant of noble metals or any sacrificial agent. The amount of H_2 obtained in CO_2 reduction was even slightly higher than that from pure water splitting. In situ DRIFT, ESR, and photoelectrochemical measurements confirmed that the highly efficient simultaneous H_2 evolution and CO_2 reduction performance was attributed to the high concentration of photogenerated electrons, separated individ-ual reactive sites as well as a unique circled electron transfer pathway E_{vb}(BiO) → E_{cb}(BiO) → E_f(RGO) → $E_{Vo\bullet}$(BiO). This study not only provides a new strategy for the development of superior heterogeneous photocatalysts for synergistic enhancement of H_2 and CH_4 evolution but also gives a deeper insight into understanding of mechanism for CO_2 reduction and water splitting.

EXPERIMENTAL SECTION

RGO-BiO QDs and pure BiO QDs. RGO-BiO QDs were prepared by the successive addition of sodium oleate (2.2 mmol) and $Bi(NO_3)_3 \cdot 5H_2O$ (0.4 mmol) to distilled water (20 mL). After vigorous stirring for 40 min, 5 mL of 1 g/L graphene oxide (GO) solution was added to the mixture. Before the suspension was transferred to a 50 mL

Teflon-lined autoclave, the volume of the precursor suspension was adjusted to 40 mL with additional distilled water. The sealed reaction system was heated at 150 °C for 16 h. The system was then allowed to cool to room temperature. The solid product obtained was collected by centrifugation, washed with absolute ethanol three times, and then freeze-dried for further characterization. For comparison, a pure BiO QDs sample was prepared without addition of the GO solution to the reaction system. The obtained precursor suspension was sealed in a 50 mL Teflon-lined autoclave up to 80% of the total volume and then heated at 140 °C for 16 h.

For comparison, TiO_2 quantum dots decorated RGO sheets were also prepared by hydrothermal synthesis according to a previous report.[38]

Characterization. The purity and the crystallinity of the as-prepared samples were characterized using powder X-ray diffraction (XRD; Rigaku RINT2500HLR+) with Cu Kα radiation at 40 kV and 80 mA. Transmission electron microscopy (TEM) analyses were performed using a JEOL JEM-2100F field emission TEM. X-ray photoelectron spectroscopy (XPS) was performed by irradiation of the sample with a 320 μm diameter spot of monochromated aluminum Kα X-rays at 1486.6 eV under ultrahigh-vacuum conditions (Ulvac Phi PHI5000VersaProbe). UV−vis diffuse reflectance spectrum spectroscopy (DRS) of the sample was measured using a Shimadzu UV-3600 UV−vis−NIR spectrophotometer. Photolumi-nescence (PL) spectra were measured with a Hitachi F-7000 fluorescence spectrophotometer at room temperature in air. Raman spectra were recorded on a Renishaw inVia Raman Microscope RE04 equipped with a 514 nm laser and a CCD camera. The Si peak at 520 cm^{-1} was used as a reference to calibrate the wavenumber. In situ diffuse reflectance infrared Fourier transform spectroscopy (DRIFT) measurements were performed on a Nicolet 8700 FTIR spectrometer using a KBr window. Prior to measurement, the catalyst powder was placed in the cell and evacuated at room temperature for 5 min. Electron spin resonance (ESR) spectra were recorded at 165 K in N_2 on a Bruker EMX 8/2.7 X-band spectrometer operated under 100 kHz modulation frequency. $^{13}CO_2$-labeled products were analyzed with GC-MS by a Shimadzu GCMS-QP2010 with thermal conductivity detector (TCD).

Photocatalytic Test. Photocatalytic CO_2 reduction experiments were performed under a 300 W Xe arc lamp placed ~10 cm from the sample. The reaction cell (capacity 600 mL) was made of Pyrex glass with a quartz window on top. A typical procedure involved 0.01 g of the as-prepared photocatalyst powder being dispersed in 100 mL of deionized water and then stirred under light irradiation. Before irradiation of the sample, high-purity CO_2 gas was slowly bubbled through the reaction vessel for 10 min. The reaction vessel was then sealed and irradiated under the Xe lamp. During the photocatalytic tests, the temperature of the reaction vessel was maintained at 4 °C by a flow of cooling water. For the water splitting experiment, pure Ar gas was slowly bubbled through the reaction vessel containing 0.01 g of catalyst and 100 mL of water for 30 min before light irradiation. The concentrations of H_2 and O_2 were determined by an online gas chromatograph equipped with a thermal conductivity detector (TCD; Ar carrier gas). The concentrations of CH_4 and CO were measured with another gas chromatograph equipped with a flame ionization detector (FID; Ar carrier gas) and a catalytic conversion furnace.

The apparent quantum efficiency (AQE) of photocatalytic CO_2 reduction was measured under the same photocatalytic reaction conditions by using 0.05 g of catalyst in 100 mL of water under a 300 nm band filter. AQE was calculated according to the following equations:

$$\text{AQE\%} = \frac{\text{no. of reacted electrons}}{\text{no. of incident photons}} \times 100\%$$

$$= \frac{2 \cdot \text{no. of evolved } H_2 + 8 \cdot \text{no. of evolved } CH_4 + 2 \cdot \text{no. of evolved CO}}{\text{no. of incident photons}} \times 100\%$$

The measurements of the number of incident photons were performed by using a calibrated silicon photodiode.

Electrochemical Measurements. Electrochemical measurements were performed on a Hokuto Denko HZ-7000 electrochemical workstation using a standard three-electrode cell with a working electrode, a platinum counter electrode, and a standard Ag/AgCl reference electrode. The working electrodes were prepared by dip coating. Briefly, 10 mg of photocatalyst was suspended in 0.15 mL of ethanol in the presence of 1% Nafion to produce a slurry, which was then dip-coated onto a 2 cm × 1.5 cm fluorine ton oxide (FTO) glass electrode and dried at 25 °C. A 300 W Xe-arc lamp was employed as a light source.

ASSOCIATED CONTENT

* Supporting Information

Detailed growth process of RGO-BiO QDs, TEM image of RGO-TiO_2 QDs, additional TEM images and XRD patterns, fluorescence lifetimes, O_2 evolution plot, GC-MS analysis of ^{13}C labeled product, photostability, in situ DRIFT spectra of CO_2 reduction on Bi_2O_3, and proposed photocatalytic process (PDF)

AUTHOR INFORMATION

Corresponding Authors

*E-mail songmeisun@i2cner.kyushu-u.ac.jp.

*E-mail ishihara@cstf.kyushu-u.ac.jp.

ORCID

Songmei Sun: 0000-0001-9545-9073

Motonori Watanabe: 0000-0003-3621-4361

Tatsumi Ishihara: 0000-0002-7434-3773

Notes

The authors declare no competing financial interest.

ACKNOWLEDGMENTS

This work received financial support from the World Premier International Research Center Initiative (WPI Initiative) on Carbon-Neutral Energy Research (I^2CNER), the Japan Ministry of Education, Culture, Sports, Science and Technol-ogy (MEXT), and grants from the National Natural Science Foundation of China (No. 21671197), from the Shanghai Science and Technology Commission (No. 16ZR1440800), and a Grant-in-Aid for Specially Promoted Research (No. 16H06293) from MEXT.

REFERENCES

(1) White, J. L.; Baruch, M. F.; Pander, J. E.; Hu, Y.; Fortmeyer, I. C.; Park, J. E.; Zhang, T.; Liao, K.; Gu, J.; Yan, Y.; Shaw, T. W.; Abelev, E.; Bocarsly, A. B. Light-Driven Heterogeneous Reduction of Carbon Dioxide: Photocatalysts and Photoelectrodes. Chem. Rev. 2015, 115, 12888.

(2) Xiang, Q.; Cheng, B.; Yu, J. Graphene-Based Photocatalysts for Solar-Fuel Generation. Angew. Chem., Int. Ed. 2015, 54, 11350.

(3) Habisreutinger, S. N.; Schmidt-Mende, L.; Stolarczyk, J. K. Photocatalytic Reduction of CO_2 on TiO_2 and Other Semi-conductors. Angew. Chem., Int. Ed. 2013, 52, 7372.

(4) Yin, G.; Nishikawa, M.; Nosaka, Y.; Srinivasan, N.; Atarashi, D.; Sakai, E.; Miyauchi, M. Photocatalytic Carbon Dioxide Reduction by Copper Oxide Nanocluster-Grafted Niobate Nanosheets. ACS Nano 2015, 9, 2111.

(5) Gao, C.; Meng, Q.; Zhao, K.; Yin, H.; Wang, D.; Guo, J.; Zhao, S.; Chang, L.; He, M.; Li, Q.; Zhao, H.; Huang, X.; Gao, Y.; Tang, Z. Co_3O_4 Hexagonal Platelets with Controllable Facets Enabling Highly Efficient Visible-Light Photocatalytic Reduction of CO_2. Adv. Mater. 2016, 28, 6485.

(6) Neatu, S.; Macia-Agullo, J. A.; Concepcion, P.; Garcia, H. Gold−Copper Nanoalloys Supported on TiO_2 as Photocatalysts for CO_2 Reduction by Water. J. Am. Chem. Soc. 2014, 136, 15969.

(7) Chang, X.; Wang, T.; Gong, J. CO_2 photo-reduction: insights into CO_2 activation and reaction on surfaces of photocatalysts. Energy Environ. Sci. 2016, 9, 2177.

(8) Gellman, A. J.; Shukla, N. Nanocatalysis: More than speed. Nat. Mater. 2009, 8, 87.

(9) Smith, A. M.; Nie, S. Semiconductor Nanocrystals: Structure, Properties, and Band Gap Engineering. Acc. Chem. Res. 2010, 43, 190.

(10) Sun, S.; Wang, W.; Li, D.; Zhang, L.; Jiang, D. Solar Light Driven Pure Water Splitting on Quantum Sized $BiVO_4$ without any Cocatalyst. ACS Catal. 2014, 4, 3498.

(11) Zhang, N.; Shi, J.; Mao, S. S.; Guo, L. Co_3O_4 quantum dots: reverse micelle synthesis and visible-light-driven photocatalytic overall water splitting. Chem. Commun. 2014, 50, 2002.

(12) Sambur, J. B.; Novet, T.; Parkinson, B. A. Multiple Exciton Collection in a Sensitized Photovoltaic System. Science 2010, 330, 63.

(13) Semonin, O. E.; Luther, J. M.; Choi, S.; Chen, H. Y.; Gao, J. B.; Nozik, A. J.; Beard, M. C. Peak external photocurrent quantum efficiency exceeding 100% via MEG in a quantum dot solar cell. Science 2011, 334, 1530.

(14) Townsend, T. K.; Browning, N. D.; Osterloh, F. E. Nanoscale Strontium Titanate Photocatalysts for Overall Water Splitting. ACS Nano 2012, 6, 7420.

(15) Tu, W.; Zhou, Y.; Liu, Q.; Yan, S.; Bao, S.; Wang, X.; Xiao, M.; Zou, Z. An In Situ Simultaneous Reduction-Hydrolysis Technique for Fabrication of TiO_2-Graphene 2D Sandwich-Like Hybrid Nano-sheets: Graphene-Promoted Selectivity of Photocatalytic-Driven Hydrogenation and Coupling of CO_2 into Methane and Ethane. Adv. Funct. Mater. 2013, 23, 1743.

(16) Li, Q.; Guo, B.; Yu, J.; Ran, J.; Zhang, B.; Yan, H.; Gong, J. R. Highly Efficient Visible-Light-Driven Photocatalytic Hydrogen Production of CdS-Cluster-Decorated Graphene Nanosheets. J. Am. Chem. Soc. 2011, 133, 10878.

(17) Li, H.; Gan, S.; Wang, H.; Han, D.; Niu, L. Intercorrelated Superhybrid of AgBr Supported on Graphitic-C_3N_4-Decorated Nitrogen-Doped Graphene: High Engineering Photocatalytic Activ-ities for Water Purification and CO_2 Reduction. Adv. Mater. 2015, 27, 6906.

(18) An, X.; Li, K.; Tang, J. Cu_2O/Reduced Graphene Oxide Composites for the Photocatalytic Conversion of CO_2. ChemSusChem 2014, 7, 1086.

(19) Xu, Y. F.; Yang, M. Z.; Chen, B. X.; Wang, X. D.; Chen, H. Y.; Kuang, D. B.; Su, C. Y. A $CsPbBr_3$ Perovskite Quantum Dot/ Graphene Oxide Composite for Photocatalytic CO_2 Reduction. J. Am. Chem. Soc. 2017, 139, 5660.

(20) Iwase, A.; Ng, Y. H.; Ishiguro, Y.; Kudo, A.; Amal, R. Reduced Graphene Oxide as a Solid-State Electron Mediator in Z-Scheme Photocatalytic Water Splitting under Visible Light. J. Am. Chem. Soc. 2011, 133, 11054.

(21) Iwase, A.; Yoshino, S.; Takayama, T.; Ng, Y. H.; Amal, R.; Kudo, A. Water Splitting and CO_2 Reduction under Visible Light Irradiation Using Z-Scheme Systems Consisting of Metal Sulfides, CoO_x-Loaded $BiVO_4$, and a Reduced Graphene Oxide Electron Mediator. J. Am. Chem. Soc. 2016, 138, 10260.

(22) Chen, Y.; Jia, G.; Hu, Y.; Fan, G.; Tsang, Y. H.; Li, Z.; Zou, Z. Two-dimensional nanomaterials for photocatalytic CO_2 reduction to solar fuels. Sus Energy & Fuels 2017, 1, 1875.

(23) Hu, S.; Lozada-Hidalgo, M.; Wang, F. C.; Mishchenko, A.; Schedin, F.; Nair, R. R.; Hill, E. W.; Boukhvalov, D. W.; Katsnelson, M. I.; Dryfe, R. A. W.; Grigorieva, I. V.; Wu, H. A.; Geim, A. K. Proton transport through one-atom-thick crystals. Nature 2014, 516, 227.

(24) Sun, S.; An, Q.; Wang, W.; Zhang, L.; Liu, J.; Goddard, W. A., III Efficient photocatalytic reduction of dinitrogen to ammonia on bismuth monoxide quantum dots. J. Mater. Chem. A 2017, 5, 201.

(25) Fu, C.; Zhao, G.; Zhang, H.; Li, S. Evaluation and Characterization of Reduced Graphene Oxide Nanosheets as Anode Materials for Lithium-Ion Batteries. Int. J. Electrochem. Sci. 2013, 8, 6269.

(26) Wang, Y. Y.; Ni, Z. H.; Yu, T.; Shen, Z. X.; Wang, H. M.; Wu, Y. H.; Chen, W.; Wee, A. T. S. Raman Studies of Monolayer Graphene: The Substrate Effect. J. Phys. Chem. C 2008, 112, 10637.

(27) Philipp, R.; Fujimoto, K. FTIR spectroscopic study of carbon dioxide adsorption/desorption on magnesia/calcium oxide catalysts. J. Phys. Chem. 1992, 96, 9035.

(28) Knöfel, C.; Martin, C.; Hornebecq, V.; Llewellyn, P. L. Study of Carbon Dioxide Adsorption on Mesoporous Aminopropylsilane-Functionalized Silica and Titania Combining Microcalorimetry and in Situ Infrared Spectroscopy. J. Phys. Chem. C 2009, 113, 21726.

(29) Seiferth, O.; Wolter, K.; Dillmann, B.; Klivenyi, G.; Freund, H.-J.; Scarano, D.; Zecchina, A. IR investigations of CO_2 adsorption on chromia surfaces: Cr_2O_3 (0001)/Cr(110) versus polycrystalline a-Cr_2O_3. Surf. Sci. 1999, 421, 176.

(30) Gabrienko, A. A.; Ewing, A. V.; Chibiryaev, A. M.; Agafontsev, A. M.; Dubkov, K. A.; Kazarian, S. G. Phys. Chem. Chem. Phys. 2016, 18, 6465.

(31) http://webbook.nist.gov/chemistry, site accessed 14 Sept, 2007.

(32) Marcano, D. C.; Kosynkin, D. V.; Berlin, J. M.; Sinitskii, A.; Sun, Z.; Slesarev, A.; Alemany, L. B.; Lu, W.; Tour, J. M. Improved Synthesis of Graphene Oxide. ACS Nano 2010, 4, 4806.

(33) Ulagappan, N.; Frei, H. Mechanistic Study of CO_2 Photo-reduction in Ti Silicalite Molecular Sieve by FT-IR Spectroscopy. J. Phys. Chem. A 2000, 104, 7834.

(34) Zhang, W.; Wang, L.; Liu, H.; Hao, Y.; Li, H.; Khan, M. U.; Zeng, J. Integration of Quantum Confinement and Alloy Effect to Modulate Electronic Properties of RhW Nanocrystals for Improved Catalytic Performance toward CO_2 Hydrogenation. Nano Lett. 2017, 17, 788.

(35) Matsumoto, Y. Energy Positions of Oxide Semiconductors and Photocatalysis with Iron Complex Oxides. J. Solid State Chem. 1996, 126, 227−234.

(36) Gao, E.; Wang, W.; Shang, M.; Xu, J. Synthesis and enhanced photocatalytic performance of graphene-Bi_2WO_6 composite. Phys. Chem. Chem. Phys. 2011, 13, 2887.

(37) Zhang, J.; Jin, Z.; Feng, C.; Yu, L.; Zhang, J.; Zhang, Z. ESR study on the visible photocatalytic mechanism of nitrogen-doped novel TiO_2: Synergistic effect of two kinds of oxygen vacancies. J. Solid State Chem. 2011, 184, 3066.

(38) Mo, R.; Lei, Z.; Sun, K.; Rooney, D. Facile Synthesis of Anatase TiO_2 Quantum-Dot/Graphene-Nanosheet Composites with En-hanced Electrochemical Performance for Lithium-Ion Batteries. Adv. Mater. 2014, 26, 2084−2088.